Available online at www.sciencedirect.com
SCIENCE DIRECT®
Advances in Space Research 37 (2006) 1950–1954
ADVANCES IN SPACE RESEARCH (a COSPAR publication)
www.elsevier.com/locate/asr

The energy spectra of protons and helium measured with the ATIC experiment

H.S. Ahn [a,*], E.S. Seo [a], J.H. Adams [b], G. Bashindzhagyan [c], K.E. Batkov [c], J. Chang [d], M. Christl [b], A.R. Fazely [e], O. Ganel [a], R.M. Gunasingha [e], T.G. Guzik [f], J. Isbert [f], K.C. Kim [a], E. Kouznetsov [c], M. Panasyuk [c], A. Panov [c], W.K.H. Schmidt [d], R. Sina [a], N.V. Sokolskaya [c], J.Z. Wang [a], J.P. Wefel [f], J. Wu [a], V. Zatsepin [c]

[a] *Institute for Physical Science and Technology, University of Maryland, CSS, Building 224, College Park, MD 20742, USA*
[b] *NASA Marshall Space Flight Center, Huntsville, AL 35812, USA*
[c] *Skobeltsyn Institute of Nuclear Physics, Moscow State University, Moscow 119899, Russia*
[d] *Max Planck Institute for Solar System Research, Katlenburg, Lindau 37191, Germany*
[e] *Department of Physics, Southern University, Baton Rouge, LA 70813, USA*
[f] *Department of Physics and Astronomy, Louisiana State University, Baton Rouge, LA 70803, USA*

Received 1 November 2004; received in revised form 9 September 2005; accepted 12 September 2005

Abstract

The Advanced Thin Ionization Calorimeter (ATIC) balloon experiment is designed to investigate the composition and energy spectra of cosmic rays at the highest energies currently accessible by direct measurements, i.e., the region up to 100 TeV. The instrument consists of a silicon matrix for charge measurement, a graphite target (0.75 nuclear interaction length) to induce hadronic interactions, three layers of scintillator strip hodoscopes for triggering and trajectory reconstruction, and a Bismuth Germanate (BGO) crystal calorimeter (18 radiation lengths) to measure particle energies. ATIC has had two successful Long Duration Balloon (LDB) flights from McMurdo, Antarctica: one from 12/28/00 to 01/13/01 and the other from 12/29/02 to 01/18/03. We present the energy spectra of protons and helium extracted from the first flight, over the energy range from 100 GeV to 100 TeV, and compare them with the results from other experiments at both the lower and higher energies. ATIC-1 results do not indicate significant differences in spectral shape between protons and helium over the investigated energy range.

Keywords: Balloon; Cosmic rays; Composition; Energy spectra

1. Introduction

ATIC is a balloon-borne experiment designed to investigate the charge and energy spectra of $Z = 1$–28 cosmic rays over the energy range from several 10s of GeV to near 100 TeV. This is an energy range in which the composition and energy spectra are not accurately known. For example, JACEE (Asakimori et al., 1998) has reported a difference in the spectral indices for protons and helium, but RUNJOB (Apanasenko et al., 2001) does not see such a difference.

ATIC has had two LDB flights from McMurdo, Antarctica, of which only the results from the first flight are presented here. The analysis of data from the second flight is still in progress, mainly due to high voltage failure on two (out of six) planes of scintillator hodoscopes that made trajectory reconstruction more difficult. The first flight accumulated 43.5 Gbytes of data that contained 26.1×10^6 cosmic ray records, 1.3×10^6 calibration records, 0.75×10^6 housekeeping records plus rate and command records (Wefel, 2001), from which calibration constants

* Corresponding author. Tel.: +1 301 405 4849; fax: +1 301 314 9363.
E-mail address: hsahn@cosmicray.umd.edu (H.S. Ahn).

0273-1177/$30
doi:10.1016/j.asr.2005.09.031

(Ahn et al., 2003b) and normalization parameters were derived.

In this paper we present energy spectra of protons and helium, along with the detailed analysis procedure.

2. ATIC experiment

2.1. ATIC instrument

The ATIC instrument has three types of detectors to measure the charge, energy and trajectory of incident cosmic rays (Guzik et al., 2004), as shown in Fig. 1. At the top of the instrument is a silicon matrix (80×56 pixels) with a total active area of 0.95×1.05 m^2 for determining the charge of incident particles (Zatsepin et al., 2004). Three layers of scintillator hodoscopes (S1, S2 and S3), interleaved with flared (24°) graphite interaction targets (T2, T3 and T4), provide a fast Pre-Trigger (PT) and help in trajectory reconstruction. S1, S2 and S3 have 42, 35 and 24 strips of dimensions $2 \times 1 \times 88.2$, $2 \times 1 \times 74.2$ and $2 \times 1 \times 52.4$ cm^3, respectively. The calorimeter consists of eight layers of 40 BGO crystals each, with each crystal $2.5 \times 2.5 \times 25$ cm^3 in size (Isbert, 2001).

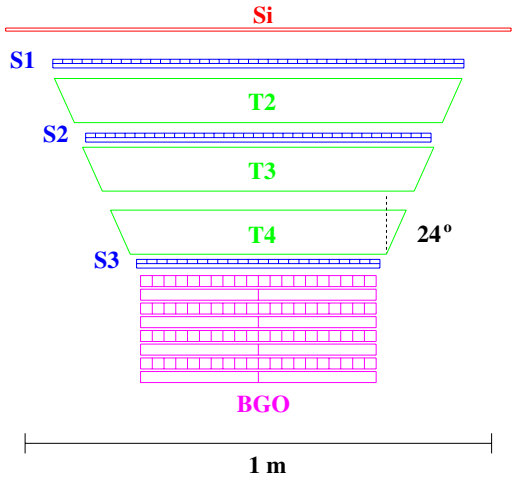

Fig. 1. ATIC instrument schematic diagram.

2.2. First flight

Before ATIC was launched, pre-flight cosmic ray muons were collected using PT (coincidence of S1 and S3) for absolute calibration of hodoscopes and calorimeter, with an average temperature of 20.9 °C. During the flight, the payload floated at an altitude of approximately 37 km, corresponding to a residual atmosphere of 4.3 g cm^{-2}, and the average temperature stayed at 25.6 ± 1.3 °C. Due to this temperature difference and the temperature dependence of BGO/PMT combination (-1.2%/°C) (Lee and Kim, 1996), the BGO calibration required a correction of 6.7% for the analysis. In-flight cosmic ray showers and helium ionization signals were also utilized for inter-range calibration of hodoscopes and calorimeter and for Si matrix calibration.

Only a subset of cosmic ray events were used for this analysis, and those events were collected with the Master Trigger (MT) in Low Energy Trigger (LET) mode, requiring 6 consecutive BGO layers to have energy greater than a given threshold in at least one crystal with PT in coincidence. The total live time (T) was estimated to be 224.2 h by: (1) summing up the time intervals during which counting for the rate records was not interrupted by other activities such as calibration or command, yielding a total of 249.1 h and (2) estimating the live time fraction using the ratio between gated and ungated MT counts from rate records (Fig. 2), providing an average of 90%.

3. Analysis

3.1. Detector response

To make the calorimeter energy deposit distribution as Gaussian as possible, good events are defined as being within the geometry and interacting near the top of the ATIC instrument. Geometry factor (GF) is calculated to be 0.24 m^2 sr by collecting only in-geometry events that pass through S1, S2, S3 and the upper 6 layers of the BGO calorimeter. Interaction probability above the second BGO layer (ε_{int}) is calculated to be 70.5% and 92.9%, respectively, for protons and helium, when the incident energy is at least

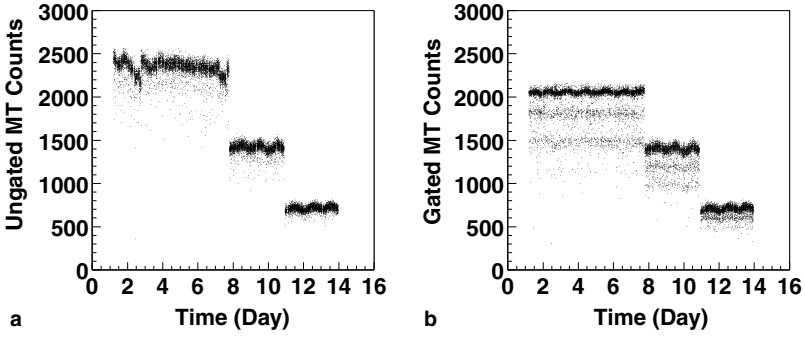

Fig. 2. Counts per minute for: (a) ungated MT and (b) gated MT, when MT was in LET mode with three different thresholds. The lighter bands in (b) are due to dead time effects.

several GeV, using the cross section parametrization in Wang et al. (2002). The interaction probability shows a slight energy dependence of $\sim(E_{\rm inc})^{0.02}$, where $E_{\rm inc}$ is the incident energy.

According to GEANT/FLUKA 3.21 simulation (Aarnio et al., 1987; Brun et al., 1984) with isotropically incident protons, the energy deposit for good events can be fitted well with a Gaussian distribution over the incident energy range of interest, with a mean energy deposit 39.1% of incident energy, and a corresponding energy resolution of 36.7%, for an incident energy of 1 TeV. The energy resolution appears to be fairly constant, while the mean energy deposit shows a slight energy dependence due to an increase in shower leakage out of the calorimeter at higher energy (Seo et al., 1996), as shown in Fig. 3. This parametrization of calorimeter response is important for the deconvolution discussed below. A superposition model was assumed to parameterize the helium response (Park, 1996).

3.2. Event selection

Several selection criteria were applied to keep high efficiency for good events while effectively reducing background events (Ahn et al., 2003a):

- The reconstructed trajectory was required to be along the shower axis to ensure the quality of trajectory reconstruction.
- The reconstructed trajectory was required to be within the fiducial volume of the ATIC instrument to remove out-of-geometry events.
- The first BGO layer was required to have less than 25% of the total energy deposit, to remove side-exit events.
- Each of the BGO layers was required to have an energy deposit larger than 125 MeV to remove non-interacting and late-interacting events.
- Of the 8 BGO layers, at least 3 even and 3 odd numbered layers were required to have more than 3% of the total energy deposit to verify sufficient energy deposit for trajectory reconstruction in both x–z and y–z.

After these selection criteria were applied to the proton simulation data, 90% of good events survived ($\varepsilon_{\rm sel}$), independent of incident energy, with a background event fraction (δ) of 5% in the selected sample at 100 GeV, and slightly higher at higher energy (9% at 100 TeV). The detection efficiency ($\varepsilon_{\rm det}$), correction for a failure of trajectory reconstruction when the incident particle passed through inactive or less active part of the detector, was estimated to be 53.2% by comparing the surviving fractions between the flight and simulation data.

For the events surviving the above selection, the particle entrance position at the Si matrix was calculated using the reconstructed trajectory, identifying the incident particle charge. Based on simulations, for the relevant energy range, the position resolution is estimated to be better than 0.5 cm (Ahn et al., 2003b), which is small compared with the Si pixel size ($2 \times 1.5\ {\rm cm}^2$).

The distribution of energy deposit was divided into 8 bins per decade, and for each bin, proton and helium candidates were separated and counted by fitting, with Landau functions, the charge distribution based on the ionization signal in the Si matrix, as shown in Fig. 4.

3.3. Deconvolution

The true counts $N_i^{\rm inc}$, in the incident energy bin i, is estimated from the measured counts $N_j^{\rm dep}$, in the deposited energy bin j, by the matrix method:

$$N_i^{\rm inc} = \frac{1}{C_i} \cdot \sum_j P_{ij} \cdot N_j^{\rm dep}, \tag{1}$$

where the matrix element P_{ij} is a probability that the events in the deposited energy bin j come from the incident energy bin i, and the compensation factor C_i is the fraction of $N_i^{\rm inc}$ that escape the selected range of energy deposit (>36.2 GeV/n), where the trigger efficiency is believed to be near 100%. They are functions of mean energy deposit, energy resolution (see Fig. 3), and an assumed initial spectral index ($\gamma_{\rm I}$). To avoid $\gamma_{\rm I}$ dependence, the procedure was repeated for many $\gamma_{\rm I}$ values, the reconstructed spectral index ($\gamma_{\rm R}$) values were compared to assumed values, selecting the ones that agreed most closely.

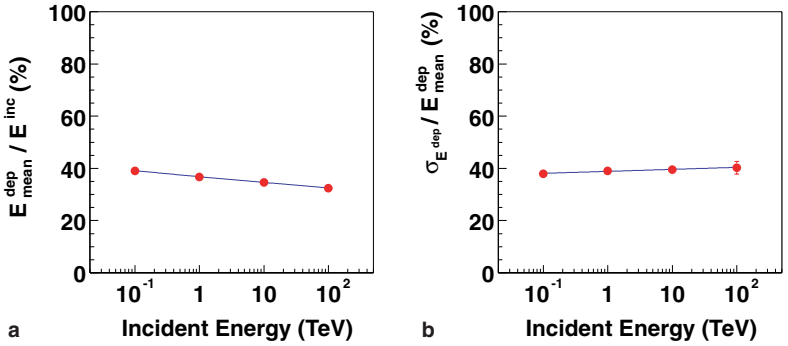

Fig. 3. ATIC calorimeter response for protons: (a) mean energy deposit ($E^{\rm dep}_{\rm mean}$) and (b) energy resolution ($\sigma_{E^{\rm dep}}/E^{\rm dep}_{\rm mean}$, where $\sigma_{E^{\rm dep}}$ is the standard deviation of the energy deposit distribution), as functions of incident energy ($E^{\rm inc}$).

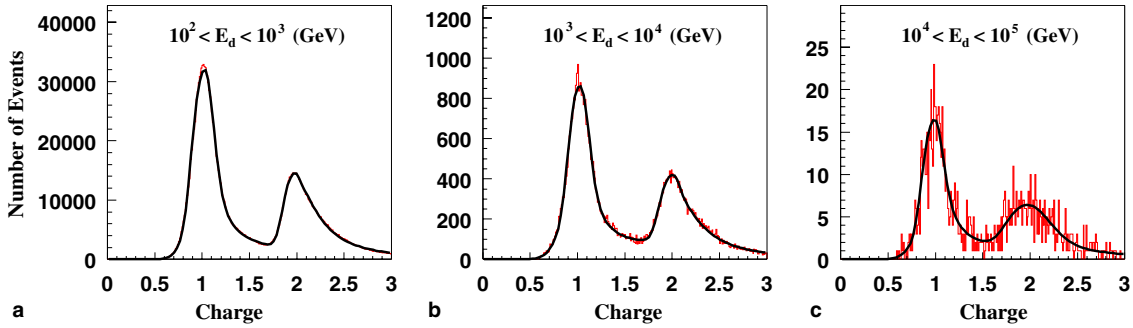

Fig. 4. Charge distributions for protons and helium from the first ATIC flight, measured by the Si matrix, after event selection, over 3 ranges of energy deposit: (a) 10^2–10^3 GeV; (b) 10^3–10^4 GeV; (c) 10^4–10^5 GeV. Fitting results used for event counting are superimposed on the distributions.

3.4. Normalization

The unfolded counts N^{inc}, in each incident energy bin of size ΔE, were normalized to obtain the differential fluxes (F) at the top of the atmosphere, given by

$$F = \frac{N^{\text{inc}}}{\Delta E} \times \frac{\beta}{\text{GF} \cdot \varepsilon_{\text{int}} \cdot \varepsilon_{\text{sel}} \cdot \varepsilon_{\text{det}} \cdot (1+\delta) \cdot T \cdot \eta}, \quad (2)$$

where most normalization parameters have been defined previously, with β being the correction for the finite energy bin size (0.99 based on γ_R values and 8 bins per decade), and with η being the correction for atmosphere attenuation loss (95% for proton and 90% for helium based on 4.3 g cm^{-2} and the angular distribution within the ATIC acceptance).

3.5. Uncertainties

Following the normalization procedure, the uncertainties of the results were estimated. A statistical error was assigned to each incident energy bin, with $\delta N_i^{\text{inc}} = \frac{1}{C_i} \cdot \Delta(\sum_j P_{ij} \cdot N_j^{\text{dep}})$, where $\Delta(\cdot\cdot)$ corresponds to 84% Poisson confidence limit (Gehrels, 1986). Several sources of systematic uncertainties were identified, including: (1) charge identification (1% for p and 3% for He); (2) BGO calibration (3%); (3) geometry factor (1%); (4) atmosphere attenuation (0.5% for p and 1.1% for He); (5) nuclear interaction probability (3% for p and 2% for He); (6) parametrization of calorimeter response (10% for p and 15% for He).

4. Results and conclusion

The proton and helium spectra at the top of the atmosphere obtained from the first ATIC flight data are shown in Fig. 5 with comparisons to other experiments (Ryan et al., 1972), AMS (Aguilar et al., 2002), CAPRICE (Boezio et al., 1999), IMAX (Menn et al., 2000) and BESS (Sanuki et al., 2000) at lower energies, and RUNJOB (Apanasenko et al., 2001) and JACEE (Asakimori et al., 1998) at higher energies. With a single LDB flight, ATIC-1 results already show a major improvement in statistics over the energy range from 0.1 to 100 TeV/n, filling a gap in the previously available data. The ATIC-1 spectra agree with magnetic spectrometer (AMS, BESS) results at low energies, and better with RUNJOB results than JACEE results at high energies. Assuming a single power law over the range investigated, proton and helium spectra were fitted with spectral indices of $2.73 \pm 0.004 \pm 0.021$ and $2.72 \pm 0.018 \pm 0.039$, respectively, with the errors being statistical and systematic, and with no indication of significant differences in spectral shape between protons and helium.

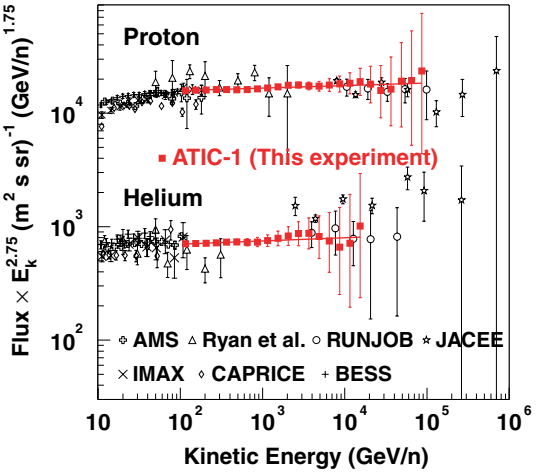

Fig. 5. Absolute differential spectra of protons and helium. Filled squares show results from the first ATIC flight. The spectra obtained by other experiments are also shown by different symbols indicated in the figure.

Acknowledgements

This work was supported by NASA grants at the University of Maryland, Marshall Space Flight Center, Southern University and Louisiana State University and by a Russian Foundation for Basic Research grant at Moscow State University.

References

Aarnio, P.A., Lindgren, J., Ranft, J., et al. Enhancements to the FLUKA86 program (FLUKA87). CERN TIS-RP-190, 1987.

Aguilar, M., Alcaraz, J., Allaby, J., et al. The alpha magnetic spectrometer (AMS) on the International Space Station: part I – results from the test flight on the space shuttle. Phys. Rep. 366, 331–405, 2002.

Ahn, H.S., Adams, J.H., Bashindzhagyan, G., et al. ATIC experiment: elemental spectra from the flight in 2000, in: Proceedings of the 28th International Cosmic Ray Conference, Tsukuba, vol. 4, pp. 1833–1836, 2003a.

Ahn, H.S., Adams, J.H., Bashindzhagyan, G., et al. ATIC experiment: flight data processing, in: Proceedings of the 28th International Cosmic Ray Conference, Tsukuba, vol. 4, pp. 2109–2112, 2003b.

Apanasenko, A.V., Sukhadolskaya, V.A., Derbina, V.A., et al. Composition and energy spectra of cosmic-ray primaries in the energy range 10^{13}–10^{15} eV/particle observed by Japanese–Russian joint balloon experiment. Astropart. Phys. 16, 13–46, 2001.

Asakimori, K., Burnett, T.H., Cherry, M.L., et al. Cosmic-ray proton and helium spectra: results from the JACEE experiment. ApJ 502, 278–283, 1998.

Boezio, M., Carlson, P., Francke, T., et al. The cosmic-ray proton and helium spectra between 0.4 and 200 GV. ApJ 518, 457–472, 1999.

Brun, R., Bruyant, F., Maire, M., et al. GEANT3. CERN DD/EE/84-1, 1984.

Gehrels, N. Confidence limits for small numbers of events in astrophysical data. ApJ 303, 336–346, 1986.

Guzik, T.G., Adams, J.H., Ahn, H.S., et al. The ATIC long duration balloon project. Adv. Space Res. 33, 1763–1770, 2004.

Isbert, J. for the ATIC collaboration. The ATIC experiment: performance of the Scintillator Hodoscopes and the BGO calorimeter, in: Proceedings of the 27th International Cosmic Ray Conference, Hamburg, vol. 6, pp. 2123–2126, 2001.

Lee, H.K., Kim, S.K. Test of BGO crystal and Hamamatsu R5611 PMT. ATIC Technical Note SNU 96-02, 1996.

Menn, W., Hof, M., Simon, M., et al. The absolute flux of protons and helium at the top of the atmosphere using IMAX. ApJ 533, 281–297, 2000.

Park, C.S. Monte Carlo simulation of high energy heavy cosmic ray primaries for the Advanced Thin Ionization Calorimeter. Master Thesis, Seoul National University, Seoul, 1996.

Ryan, M.J., Ormes, J.F., Balasubrahmanyan, V.K. Cosmic-ray proton and helium spectra above 50 GeV. Phys. Rev. Lett. 28, 985–988, 1972.

Sanuki, T., Motoki, M., Matsumoto, H., et al. Precise measurement of cosmic-ray proton and helium spectra with the BESS spectrometer. ApJ 545, 1135–1142, 2000.

Seo, E.S., Adams, J.H., Bashindzhagyan, G., et al. The Advanced Thin Ionization Calorimeter (ATIC) experiment: expected performance, in: Proceedings of SPIE International Symposium on Optical Science, Engineering, and Instrumentation 2806, 134–144, 1996.

Wang, J.Z., Seo, E.S., Anraku, K., et al. Measurement of cosmic-ray hydrogen and helium and their isotopic composition with the BESS experiment. ApJ 564, 244–259, 2002.

Wefel, J.P. for the ATIC collaboration. The ATIC experiment: first balloon flight, in: Proceedings of the 27th International Cosmic Ray Conference, Hamburg, vol. 5, pp. 2111–2114, 2001.

Zatsepin, V.I., Adams, J.H., Ahn, H.S., et al. The silicon matrix as a charge detector in the ATIC experiment. Nucl. Instrum. Meth. A 524, 195–207, 2004.